

Accepted Manuscript

LIBS and ablation threshold analysis using a megahertz Yb fiber laser oscillator

Gregory J. Parker, Daniel E. Parker, Bai Nie, Vadim Lozovoy, Marcos Dantus

PII: S0584-8547(15)00059-2
DOI: doi: [10.1016/j.sab.2015.02.011](https://doi.org/10.1016/j.sab.2015.02.011)
Reference: SAB 4871

To appear in: *Spectrochimica Acta Part B: Atomic Spectroscopy*

Received date: 25 March 2014
Revised date: 12 October 2014
Accepted date: 20 February 2015

Please cite this article as: Gregory J. Parker, Daniel E. Parker, Bai Nie, Vadim Lozovoy, Marcos Dantus, LIBS and ablation threshold analysis using a megahertz Yb fiber laser oscillator, *Spectrochimica Acta Part B: Atomic Spectroscopy* (2015), doi: [10.1016/j.sab.2015.02.011](https://doi.org/10.1016/j.sab.2015.02.011)

This is a PDF file of an unedited manuscript that has been accepted for publication. As a service to our customers we are providing this early version of the manuscript. The manuscript will undergo copyediting, typesetting, and review of the resulting proof before it is published in its final form. Please note that during the production process errors may be discovered which could affect the content, and all legal disclaimers that apply to the journal pertain.



LIBS and ablation threshold analysis using a megahertz Yb fiber laser oscillator

Gregory J. Parker¹, Daniel E. Parker¹, Bai Nie¹, Vadim Lozovoy¹, and Marcos Dantus^{1,2}

¹Department of Chemistry, Michigan State University, East Lansing, Michigan 48824, United States

²Department of Physics and Astronomy, Michigan State University, East Lansing, Michigan 48824, United States

Email: dantus@msu.edu, Phone: 517-355-9715 ext. 315

Abstract

A LIBS system is demonstrated using a 100m cavity Yb fiber oscillator producing ~ 70 ps, 320nj clusters of 50-100fs sub-pulses at 2MHz. A new empirical model for femtosecond ablation is presented to explain the LIBS signal intensity's non-linear dependence on pulse fluence by accounting for the Gaussian beam's spatial distribution. This model is compared to experimental data and found to be superior to linear threshold fits. This model is then used to measure the ablation threshold of Cu using a typical amplified Ti:Sapphire system, and found to reproduce previously reported values to within $\sim 20\%$. The ablation threshold of Cu using the Yb fiber oscillator system was measured to be five times lower than on the amplified Ti:Sapphire system. This effect is attributed to the formation of nanostructures on the surface, which have previously been shown to decrease the ablation threshold. The plasma lifetime is found to be ~ 1 ns, much shorter than that of nanosecond ablation, further indicating that the decreased threshold results from surface effects rather than laser-plasma interaction. The low threshold and high pulse energy of the Yb fiber oscillator allows the acquisition of LIBS spectra at megahertz repetition rates. This system could potentially be developed into a compact, fiber-based portable LIBS device taking advantage of the benefits of ultrafast pulses and high repetition rates.

1. Introduction

Since its introduction, laser-induced breakdown spectroscopy (LIBS) has become a valuable tool for determining atomic composition in analytical spectroscopy because it is virtually instantaneous, highly sensitive, and requires no sample preparation [1]. LIBS has been successfully applied to analyze the composition of a wide variety of materials, including products in the steel industry [2,3], works of art and archaeological artifacts [4], terrestrial and Martian geological samples [5,6], and toxic materials [7,8]. Briefly, the LIBS mechanism works by focusing a short laser pulse onto a sample, ablating a small amount of material and forming a plasma plume. Electron transitions between bound states in the ablated atoms and ions radiate at characteristic atomic emission frequencies, which can be collected and identified with a spectrometer to determine atomic composition.

Much of the recent work in LIBS has been driven by the need for portable systems for use outside the laboratory [9]. Many existing portable and laboratory LIBS systems employ solid-state nanosecond lasers (e.g. Nd:YAG) with pulse energies in the millijoule range. Several characteristics of these systems make them less than ideal to incorporate into compact and robust portable devices. First, because nanosecond ablation is an inefficient thermal process, it requires high pulse energies to achieve reasonable sensitivity and results in atomic emissions accompanied by a spectrally broad continuum emission that can require a gated spectrometer to eliminate. Second, solid-state lasers are often large, and sensitive to vibration and ambient conditions. In recent years, the development of fiber laser technology has offered a promising alternative laser source for use in portable devices. Fiber lasers are generally more stable, smaller, and more efficient than their solid-state counterparts. Additionally, they require no cooling, have excellent beam quality, and can easily deliver high average power, all of which make them ideal for application outside the laboratory.

Independent of the type of laser used for LIBS, several advantages have been observed when replacing nanosecond pulses with femtosecond pulses. Ultrafast pulses lower the ablation threshold, and therefore the required pulse energy, as well as significantly reducing the continuum radiation by delivering energy on a timescale orders-of-magnitude faster than thermal effects [10,11]. Ultrafast pulses also offer additional advantages such as matrix independence, ambient pressure independence, and high spatial resolution [12,13]. These advantages make ultrafast pulses ideal in situations where delicate sampling is required (i.e. high spatial resolution, less sample destruction). Fiber-based and ultrafast fiber-based LIBS have been successfully demonstrated in the laboratory [14-16] but, to the authors' knowledge, no portable commercial ultrafast LIBS devices are yet available.

When performing LIBS with ultrafast pulses, energy considerations become crucial because ultrafast pulses generally deliver far lower energy (number of photons) than nanosecond ones. This demands that ultrafast LIBS systems include amplifiers to reach pulse energies necessary for ablation, which significantly increases their size, weight, and power consumption requirements. If the need for amplifiers could be eliminated, femtosecond fiber-based LIBS systems could potentially be designed to rival nanosecond ones for portability. The elimination of the amplifier, however, forces such systems to operate with pulse fluences near the ablation threshold.

In recent years, atomistic molecular dynamics simulations for femtosecond laser ablation have improved significantly [17, 18], giving new insights into the ablation process for ultrafast pulses. This new understanding can be used to improve the operation of an ultrafast fiber oscillator for LIBS. Laser fluences near the ablation threshold lead to the creation of laser-induced periodic surface structures (LIPSS), first observed in 1965 [19] and confirmed as a

universal phenomenon in 1982 [20]. The structures usually take the shape of gratings with a spacing that ranges from the wavelength of the incident photons to five times shorter than the wavelength. The structures result in reduced reflectivity and a decrease in ablation threshold [21]. The mechanism for LIPSS formation involves a non-thermal process known as nanostructuring, whereby transient intrapulse interference occurs between an incident pulse and a transient surface plasmon wave (plasma) induced by a previous laser pulse [20]. The number of pulses influences the size of the nanometer features, the larger the number of pulses the smaller the features [22]. Nanometer structure formation depends exponentially on the timing between the laser pulses; near the threshold, the $1/e$ time varies from 0.78ps for titanium to 0.14ps for SiO₂ [23]. Therefore, shorter time delays lead to greater surface area being covered by LIPSS, and one can expect greater LIBS signal. The greater the number of pulses, the lower the threshold for non-thermal nanostructuring and even ablation [24].

In this study, a Ytterbium fiber oscillator is used for LIBS at near-threshold fluences. This laser satisfies important qualities for LIBS analysis including (a) the presence of femtosecond pulses required for non-thermal nanostructuring, (b) multiple pulses separated by times shorter than 0.5ps to yield high frequency LIPSS formation, and (c) a combination of MHz repetition rate and nanojoule pulse energies not typically used for LIBS. An empirical model of laser ablation that allows measurement of the ablation threshold is presented and compared to experimental data. LIBS is then demonstrated using a Yb fiber oscillator and both the evidence for and the implications of multi-pulse effects are discussed.

2. Experimental Setup

The LIBS system uses a Yb-doped ultrafast fiber oscillator as pulse source. This oscillator uses only single mode fibers of 10 μ m core diameter and produces pulses with a broad, roughly-Gaussian spectrum centered at 1070nm with a FWHM of \sim 35nm (Fig. 1c). The laser has an all-normal dispersion cavity with 10/125 μ m double-clad Yb doped gain fiber. Mode-locking is based on a nonlinear pulse evolution mechanism. This cavity is unusually long, with more than 100m passive single-mode fiber, which results in a repetition rate of 2MHz. Due to the large dispersion and nonlinearity introduced by the long fiber, the laser operates in an unusual mode that delivers 70ps pulse clusters consisting of numerous femtosecond sub-pulses (Fig. 1d). Each sub-pulse is estimated to have \sim 50-100fs pulse duration, but with random delay from other sub-pulses. The output energy of a single pulse cluster can be up to 320nJ. Detailed analysis of the oscillator's mode of operation can be found in [25].

The output beam is collimated with a telescope before being directed to the LIBS setup, as shown in Figure 1a. The beam is focused onto the sample using a 20x objective (Nikon, Plan Fluor ELWD, NA=0.45). The beam diameter is measured at \sim 5 μ m ($1/e^2$ diameter) at the focal plane. Samples are mounted on a spinning wheel (\sim 130Hz) to get fresh ablation spots, and translation stages are used to adjust the sample's position and angle relative to the incident beam. Accurate placement of the sample in the beam focus was crucial due to the use of near-threshold pulse fluences. Ablation could only be achieved in a \sim 1mm region of the beam path around the focal point. To obtain spectra, the sample is tilted at 45° relative to the incoming beam, and 400 μ m collection fiber is placed \sim 1cm from the sample, resulting in a collection angle of 10^{-4} sr. When measuring the strength of the LIBS signal, the sample is placed perpendicular to the

oncoming beam, and radiation from the plasma is collected along the incident beam path by placing a wavelength dependent beam splitter between the second collimating lens and the objective then focusing into the same collection fiber. This alternative setup results in a collection angle of 0.67sr , but greatly attenuates wavelengths below 350nm due to glass optics. A small fiber coupled spectrometer (USB4000, Ocean Optics, $178\text{-}876\text{nm}$) was used to record the LIBS signal. This spectrometer was chosen with portability in mind, in contrast to larger, much more sensitive and higher resolution spectrometers traditionally used for LIBS, though it limits resolution to $\sim 1.2\text{nm}$.

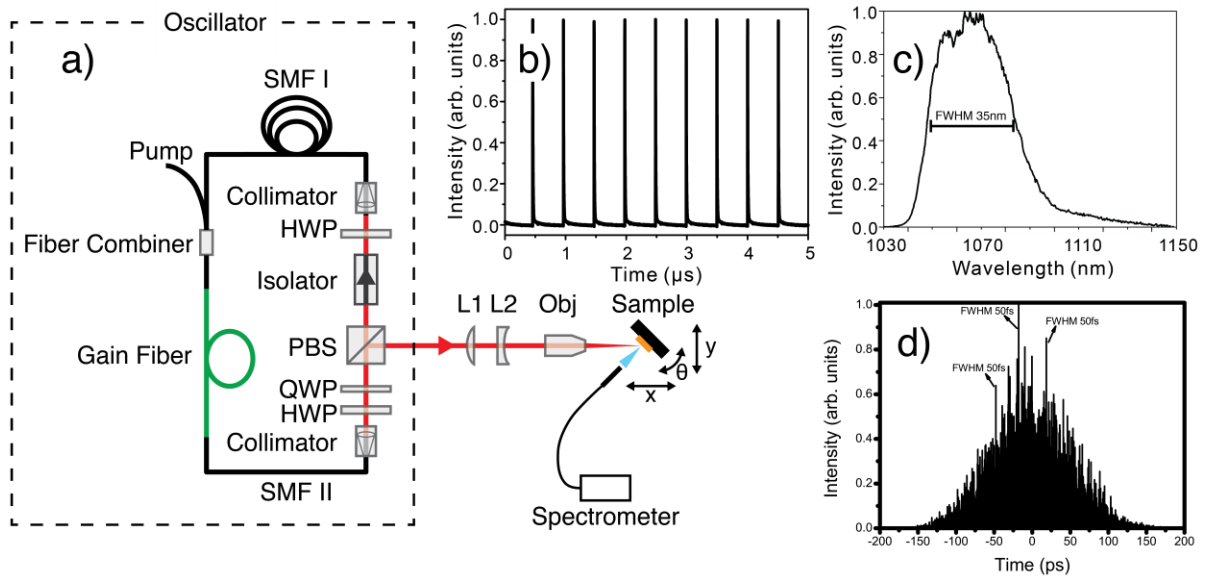


Figure 1: a) Experimental setup of the fiber laser oscillator and LIBS detection. SMF, single mode fiber; HWP and QWP, half- and quarter-wave plates; PBS, polarization beam splitter; L1 and L2, lenses to collimate the output beam; Obj, objective lens. b) 2MHz pulse train. c) Pulse spectrum. d) simulated femtosecond pulse cluster consistent with the laser parameters and measured autocorrelation which averages millions of different pulse clusters [25].

3. LIBS Threshold and Modeling

The dependence of the LIBS signal on pulse fluence is studied to understand the behavior of the LIBS signal at near-threshold fluences. It is observed that the dependence is slightly non-linear at these fluences. This refines a previously used model, which proposed the intensity of the LIBS signal for a femtosecond pulse depends linearly on pulse fluence once the threshold value is reached [26]. In other words, the LIBS signal strength was previously assumed to be linear with laser fluence and given by

$$\text{LIBS}(\Phi) = \begin{cases} 0 & \text{if } \Phi < F_{\text{Th}} \\ k(\Phi - F_{\text{Th}}) & \text{if } \Phi > F_{\text{Th}} \end{cases}, \quad (1)$$

where Φ is the pulse fluence, F_{Th} is the ablation threshold, and k is a constant of proportionality. The value of the ablation threshold has formerly been measured from experimental data using a linear fit with Equation (1).

Considering the spatial distribution of the laser beam leads to a more accurate model. Intuitively, since the laser beam intensity distribution is spatially Gaussian, ablation first occurs in a small region in the center of the beam where peak fluence locally exceeds the threshold. As the pulse energy further increases, both the intensity of ablation and the area ablated increase. Once the pulse energy is high enough that almost all of the focal spot contributes to the ablation, the LIBS signal intensity increases almost linearly with total pulse fluence. The resulting non-linearity of the LIBS signal can cause substantial errors in threshold value measurements when using a linear approximation. Figure 2 gives a cartoon depiction of the ablated area and the resulting LIBS signal strength as the laser intensity is increased. A hypothetical linear fit is shown to demonstrate how assuming linearity could cause measurement error. Below, we present a model that accounts for this non-linearity and allows for more accurate measurements of the threshold.

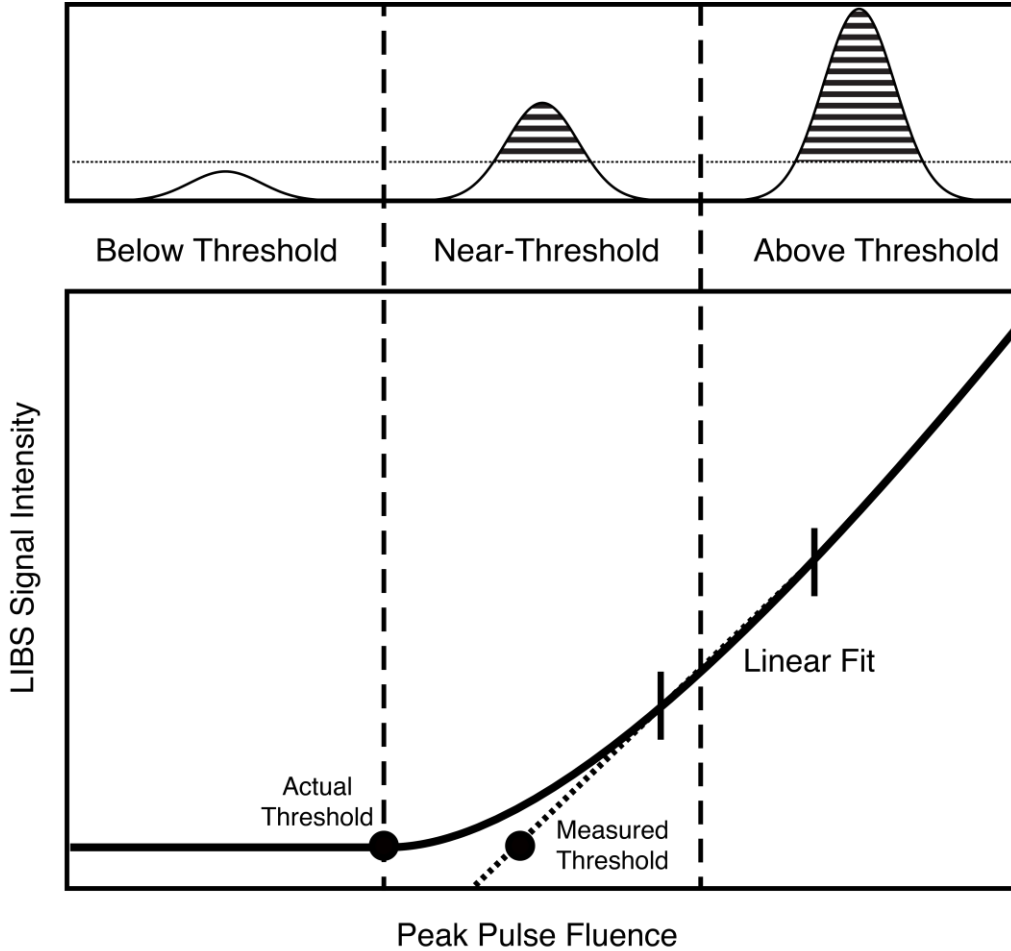


Figure 2: Cartoon diagram of ablation and LIBS signal as a function of laser fluence. (Top) The spatial fluence distribution in three different regimes: below the ablation threshold, the non-linear regime just above the threshold, and the nearly-linear regime far above the threshold. The shaded region corresponds to the portion of the pulse that exceeds the ablation threshold (dotted line), and therefore contributes to the LIBS signal. (Bottom) The simulated LIBS signal based on the model presented in Eq. (2) with a potential linear fit between the vertical bars and the resulting error shown.

Our model assumes that the linear dependence of the LIBS signal on pulse fluence (Eq. 1) holds separately at each point on the surface. That is, at each point on the sample, ablation does not occur until the local fluence rises above the threshold, after which the amount of ablation is proportional to the fluence above the threshold level. The total dependence of the LIBS signal on pulse fluence is therefore obtained by integrating over the focal spot in the spatial domain. The beam is assumed to be spatially Gaussian and perpendicular to the sample. Therefore, the pulse fluence incident on the surface of the sample is given by $\Phi(r, \theta) = \Phi_0 \exp(-r^2/2\sigma^2)$ where σ is the standard deviation of the Gaussian beam and Φ_0 is the peak pulse fluence, which is related to the pulse energy E by $\Phi_0 = \frac{E}{\pi\sigma^2}$. For a Gaussian beam, the peak pulse fluence is exactly twice the average fluence.

The total LIBS signal as a function of pulse fluence is therefore given by integrating Eq. (1) over the focal spot:

$$\text{LIBS}_{\text{Total}}(\Phi) = \int_0^{2\pi} \int_0^{r_0} k[\Phi e^{-r^2/2\sigma^2} - F_{\text{Th}}] r dr d\theta = \begin{cases} 0 & \text{if } \Phi < F_{\text{Th}} \\ k[\Phi - F_{\text{Th}} + F_{\text{Th}} \ln(F_{\text{Th}}/\Phi)] & \text{if } \Phi > F_{\text{Th}} \end{cases}, (2)$$

where Φ is the pulse fluence, F_{Th} is the ablation threshold, k is a constant of proportionality, and r_0 is the radius at which $\Phi = F_{\text{Th}}$. This equation is almost identical to Eq. (1), but contains a correctional logarithmic term. The effect of this term is that, near the threshold, both the intensity of the LIBS signal and its derivative increase. At higher fluences, the derivative approaches a constant.

This non-linearity is the source of the aforementioned error from using linear extrapolation to measure the threshold. If the LIBS signal is measured at large fluence values in

the nearly-linear regime, then a linear extrapolation will yield a threshold value higher than the real one. Moreover, the larger the fluence values used in the extrapolation, the larger the error will be. A more accurate method is to use F_{Th} and k as fitting parameters and to then perform a non-linear fit with Eq. (2) to determine the threshold. This is carried out below on experimental data.

4. Experimental Results

Measurements of the ablation threshold were carried out by varying laser power and recording the total intensity of the LIBS spectrum. Total intensity was taken to be the integrated intensity across all wavelengths, and thus included the continuum radiation as well as spectral emissions. Both the Yb fiber oscillator described above and an amplified Ti:Sapphire setup (Legend USP, Coherent) producing pulses of ~ 35 fs at 1kHz were tested [26,27]. All experiments were performed in temperature and humidity controlled laboratories (291K, 1 atm, 30-40% relative humidity). Experimental data are compared with the model discussed above (Fig 3), and found to be in agreement, including the region near the threshold where a linear fit visibly deviates from data (Fig. 3b). The fiber oscillator employs single-mode fibers, ensuring the validity of assuming a Gaussian spatial profile. On the Ti:Sapphire setup, a beam profiler (Coherent) was used to validate this assumption (Fig. 3d). Using the amplified setup, a fit using Eq. (2) results in a measured threshold value for copper of $F_{Th} \sim 1.25 \text{ J/cm}^2$ peak pulse fluence (Fig. 3a,b), which corresponds to $\sim 0.63 \text{ J/cm}^2$ average pulse fluence, in rough agreement with previously measured values for the threshold of copper of 0.49 J/cm^2 (Momma et al.) and 0.55 J/cm^2 (Gunaratne et al.) using femtosecond pulses in vacuum and at 1atm, 291K, 30-40% relative humidity respectively [28, 27].

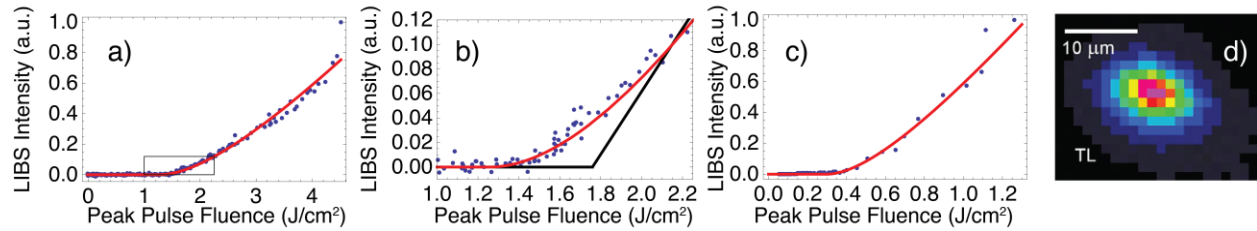


Figure. 3: Comparison of LIBS signal strength simulations with experimental data obtained for copper. a) Both linear (Eq. 1) and logarithmic (Eq. 2) equations fit to data from the amplified laser system. b) close-up of threshold region, as indicated by dashed box in a). c) Logarithmic equation fit to data from fiber oscillator. d) Spatial beam profile of the amplified Ti:Sapphire laser system at the focal plane.

Using the Yb fiber laser, the ablation threshold of copper was found to be $\sim 0.13 \text{ J/cm}^2$ average pulse fluence ($\sim 0.25 \text{ J/cm}^2$ peak pulse fluence). This is surprisingly only about one fifth of the threshold found using the Ti:Sapphire setup. The lower threshold found for the Yb laser is attributed to the multi-pulse effects from the clusters of femtosecond pulses produced by the oscillator. One possible explanation of these results is the creation of LIPSS. LIPSS have been shown to alter the surface morphology in such a way as to decrease reflectivity and thereby decrease ablation the threshold [21]. Additionally, the formation of LIPSS depends exponentially on the delay time between pulses with a $1/e$ decay time on the order of hundreds of femtoseconds. [23]. Here, with the fiber oscillator producing $\sim 70\text{ps}$ pulses consisting of clusters of many 50fs sub-pulses with separation $< 500\text{fs}$, one can expect extensive nanostructuring and a decreased ablation threshold.

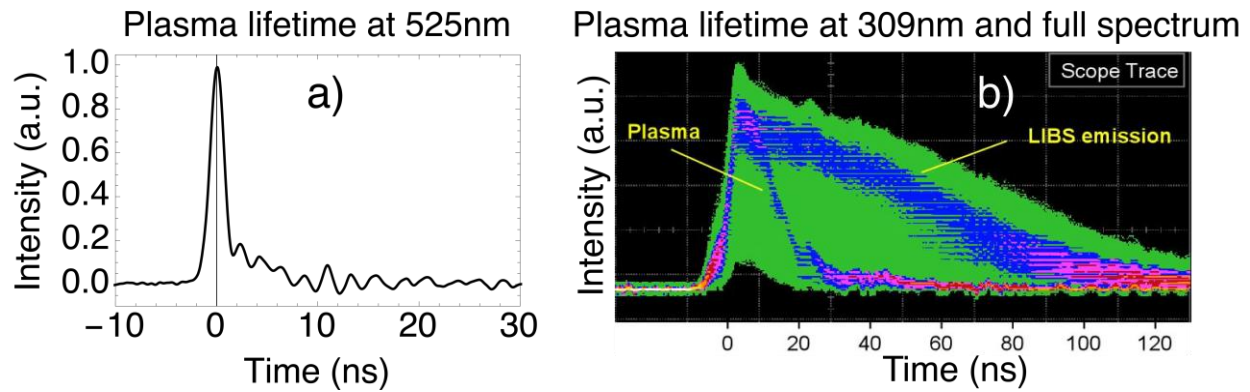


Figure 4: a) The plasma lifetime measured for the Yb fiber oscillator on aluminum. b) The plasma lifetime measured for the Ti:Sapphire setup on aluminum, and the LIBS emission lifetime of the 309.3 nm aluminum line, which was found to be ~80ns, in good agreement with the recorded value of 81ns (NIST database).

The recorded plasma emission lifetime ($1/e$) was measured at ~1ns (Fig. 4a), which is shorter than the lifetime for typical femtosecond LIBS using an amplified setup; measured at 15-20ns (Fig. 4b). These measurements were carried out by placing a PMT (2ns rise time, 3ns decay) behind a monochromator and connecting the PMT output (with 50 Ω termination) to a digital oscilloscope. Both these values for the plasma lifetimes are shorter than those recorded for nanosecond LIBS, which typically range from hundreds of nanoseconds to several microseconds. This is in agreement with previous comparisons of femtosecond and nanosecond plasma lifetimes [29]. The shorter lifetime found for the fiber oscillator is likely a result of the low pulse energy. The measured lifetime for the Yb oscillator is far less than the 500ns delay between the clusters of pulses it produces, indicating that the observed decrease in ablation threshold is more likely due to a surface effect from short delays between sub-pulses such as LIPSS rather than pulse clusters interacting with the plasma of previous clusters.

It should be noted that the decrease in ablation threshold is in contrast to multi-pulse effects observed for nanosecond ablation. When nanosecond pulses are employed for ablation at high repetition rates (e.g. $>10^4$ Hz) the melted surface area resulting from one pulse does not have sufficient time to re-solidify before the next pulse hits. The subsequent pulses therefore encounter a liquid with a higher ablation threshold than the same material in solid phase, resulting in a higher overall ablation threshold. It is therefore not advantageous in the nanosecond regime to use laser sources operating at higher repetition rates but lower pulse energies, such effort leads to decreased LIBS signal [30,31].

With the Yb fiber oscillator, the negative effects of high repetition rates are eliminated. The decreased ablation threshold leads to clear LIBS spectra at relatively low fluences with easily identifiable emissions peaks in good correspondence with known atomic emissions (NIST database). The spectra of copper and brass (approx. 70% copper, 30% zinc) are compared in Figure 5. In the brass spectrum, zinc peaks are visible (e.g. 330.3, 334.5, 472.2, and 481.1nm) which are absent in the copper spectrum. The emission peaks of copper at (e.g. 324.8, 327.4, 510.5, 515.3, and 521.8nm) appear in both spectra.

The sensitivity of the system, while worse than that of powerful LIBS systems designed for low limits of detection, is surprising considering spectra are taken at fluences of <0.75 J/cm² average pulse fluence (<1.5 J/cm² peak pulse fluence), very near, or even below the ablation threshold on typical laser systems and with <300 ms collection. The resulting total energy for each spectrum is approximately 80mJ. Single spectra have a signal-to-noise ratio of approximately 130:1. All spectra are taken at room temperature (291K), atmospheric pressure, and relative humidity of 30-40%. To assess the limits of the system's sensitivity, the spectra of three different industrial aluminum alloys (Al 1100, Al 6061, Al 7075) are compared (Fig. 6).

The three alloys differ by concentrations on the order of 1%. Al 6061 contains 0.8-1.2% Mg, which is visible in small Mg peaks (278.3, 285.2, 383.8, 518.4nm). Al 7075 contains a higher (2.1-2.9%) concentration of Mg, 1.2-2% Cu, and 5.1-6.1% Zn (visible at 324.8, 327.4nm, and 330.3 and 334.5nm respectively). It is unclear why the emissions from zinc and copper are so weak in this spectrum. The precision in the measurement of Mg concentration is estimated to be ~0.2% by linearly extrapolating the peak heights' dependence on concentration until they fall below twice the noise level. Quantitative concentration measurements would require calibration of the system with a variety of samples and concentrations, such as done by Clegg *et al.* [32]. In addition to smooth metallic samples, a natural Galena (PbS) rock with a rough surface is also tested. Strong Pb emissions can be observed (e.g. 364.0, 368.3, and 405.8nm), as shown in Figure 7. In contrast to metallic samples, this sample was not translated as spectra were taken. This result demonstrates that spectra can be obtained from a sample before the ablation process alters the surface morphology enough to significantly decrease signal strength, even in the absence of sample translation or beam scanning.

The low threshold from multi-pulse effects and the absence of interfering thermal effects from using ultrafast pulses eliminates the disadvantages of driving the laser into a regime with high repetition rate but low pulse energy. This makes the Yb oscillator's mode of operation a viable candidate for a LIBS system without the need for amplifiers that decrease repetition rate in favor of pulse energy. It should not be forgotten, however, that this oscillator's mode of operation is by no means standard. A typical oscillator producing pulses of only a few nanojoules would fail to reach fluences necessary for ablation at all. This oscillator's unique mode of operation producing pulse bursts of up to 320nj is therefore crucial. With improved sensitivity and sufficient engineering to reduce size, weight, and power consumption, this system could

conceivably be used in a portable LIBS device for real-time analysis. With existing technology, the entire system could be reduced to a size of $\sim 0.1\text{m}^3$ and $\sim 10\text{kg}$, with a power requirement of less than 30W.

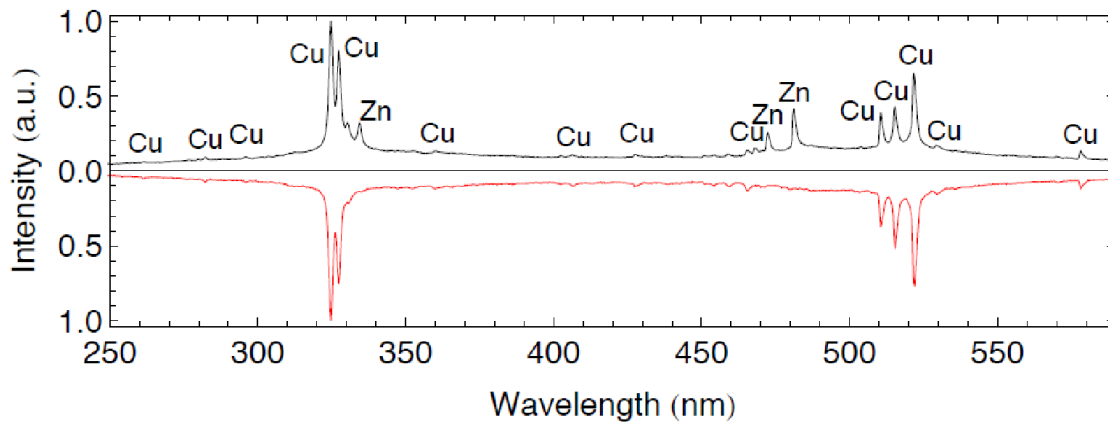


Figure 5: A comparison of the LIBS spectra of Brass (Top) and Copper (Bottom) obtained with the Yb oscillator. The spectra were both collected in single $\sim 150\text{ms}$ exposure without time gating or other type of filtering.

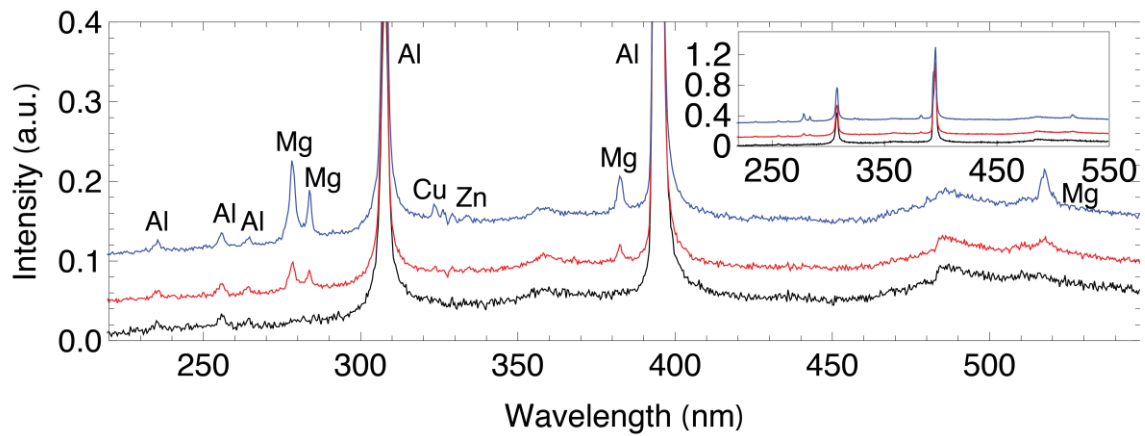


Figure 6: A comparison of three alloys of Aluminum (vertically offset for clarity): Al 1100 (bottom), Al 6061 (middle), and Al 7075 (top). Spectra are offset for clarity. Inset: full range of same spectra.

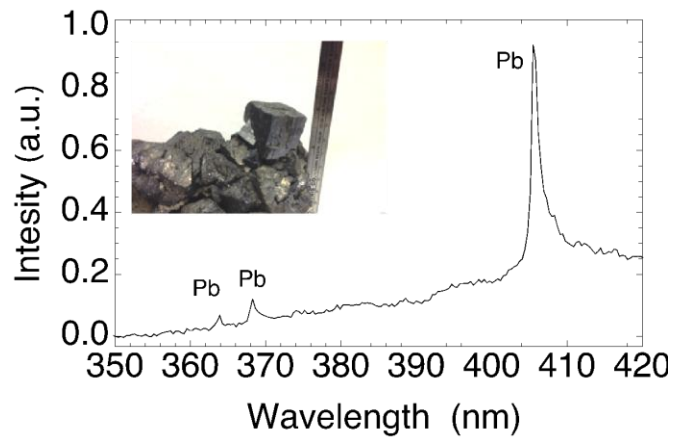


Fig. 7: Use of the Yb oscillator to examine the mineral content of a rock. A close-up view of the lead atomic lines present in the LIBS spectrum obtained from a Galena (PbS) rock sample (inset, approximately 10cm tall).

5. Conclusions

A LIBS system has been demonstrated using a 100m cavity Yb fiber oscillator with a unique mode of operation producing ~ 70 ps, 320nj clusters of 50fs sub-pulses at 2MHz. A new empirical model for femtosecond ablation was presented to explain the non-linearity of the LIBS signal intensity's dependence on pulse fluence by accounting for the Gaussian beam's spatial distribution. This model was compared to experimental data and found to agree better than simple linear fits. This model was then used to measure the ablation threshold of Cu using a typical amplified Ti:Sapphire system, and found to reproduce previously reported values to within $\sim 20\%$.

The ablation threshold of Cu on the Yb fiber oscillator system was measured to be five times lower than on the amplified Ti:Sapphire system. This effect is attributed to the formation of nanostructures (LIPSS) on the surface, which have previously been shown to decrease the ablation threshold. The plasma lifetime is found to be ~ 1 ns, much shorter than that of nanosecond ablation, further indicating that the decreased threshold results from surface effects rather than laser-plasma interaction. The low threshold and high pulse energy of the Yb fiber oscillator allows the acquisition of LIBS spectra in a new regime of megahertz repetition rates combined with several hundred nanojoule pulse energies. The LIBS spectra obtained demonstrate surprising sensitivity considering the use of energies very near or even under the threshold reported for other ultrafast laser systems. Perhaps most importantly, this low threshold and high oscillator pulse energy renders the use of amplifiers unnecessary. For this reason, the system demonstrated here could be developed into a compact, fiber-based portable LIBS device taking advantage of the benefits of ultrafast pulses and high repetition rates.

Acknowledgements

We gratefully acknowledge funding from an Early-concept Grant for Exploratory Research NSF 1014538, Tanja Pietraß program officer. We also thank the High School Honors Science Mathematics Engineering Program at Michigan State University led by Gail Richmond and the Okemos Honors Research Program lead by Andrew Moore for supporting Gregory Parker.

References

- [1] J.P. Singh, S.N. Thakur (Eds.). Laser-induced breakdown spectroscopy. Elsevier (2007).
- [2] R. Noll, H. Bette, A. Brysch, M. Kraushaar, I. Mönch, L. Peter, V. Sturm. Laser-induced breakdown spectrometry—applications for production control and quality assurance in the steel industry. *Spectrochimica Acta Part B: Atomic Spectroscopy*, 56(6) (2001), 637-649.
- [3] J. Gruber, J. Heitz, H. Strasser, D. Bäuerle, N. Ramaseder. Rapid in-situ analysis of liquid steel by laser-induced breakdown spectroscopy. *Spectrochimica Acta Part B: Atomic Spectroscopy*, 56(6) (2001), 685-693.
- [4] D. Anglos. Laser-Induced Breakdown Spectroscopy in Art and Archaeology. *Appl. Spectrosc.*, 55(6) (2001), 186A-205A .
- [5] J. Cunat, S. Palanco, F. Carrasco, M.D. Simon, J.J. Laserna. Portable instrument and analytical method using laser-induced breakdown spectrometry for in situ characterization of speleothems in karstic caves. *Journal of Analytical Atomic Spectrometry*, 20(4) (2005), 295-300.
- [6] A.K. Knight, N.L. Scherbarth, D.A. Cremers, M.J. Ferris. Characterization of laser-induced breakdown spectroscopy (LIBS) for application to space exploration. *Applied Spectroscopy*, 54(3) (2000), 331-340.
- [7] F. Capitelli, F. Colao, M.R. Provenzano, R. Fantoni, G. Brunetti, N. Senesi. Determination of heavy metals in soils by laser induced breakdown spectroscopy. *Geoderma*, 106(1) (2002), 45-62.
- [8] J.L. Gottfried, F.C. De Lucia Jr., C.A. Munson, A.W. Miziolek. Laser-induced breakdown spectroscopy for detection of explosives residues: a review of recent advances, challenges, and future prospects. *Analytical and bioanalytical chemistry*, 395(2) (2009), 283-300.
- [9] J. Rakovský, P. Čermák , O. Musset , P. Veis. A review of the development of portable laser induced breakdown spectroscopy and its applications. *Spectrochimica Acta Part B: Atomic Spectroscopy*, 101 (2014), 269-287.

- [10] V. Margetic, A. Pakulev, A. Stockhaus, M. Bolshov, K. Niemax, R. Hergenröder. A comparison of nanosecond and femtosecond laser-induced plasma spectroscopy of brass samples. *Spectrochimica acta part B: Atomic spectroscopy*, 55(11) , 1771-1785.
- [11] M. Baudalet, L. Guyon, J. Yu, J.P. Wolf, T. Amodeo, E. Fréjafon, P. Laloi. Femtosecond time-resolved laser-induced breakdown spectroscopy for detection and identification of bacteria: A comparison to the nanosecond regime. *J. Appl. Phys.* 99(8) (2006), 084701.
- [12] R.E. Russo, X.L. Mao, C. Liu, J. Gonzalez. Laser assisted plasma spectrochemistry: laser ablation. *J. Anal. At. Spectrom.* 19(9) (2004), 1084-1089.
- [13] V. Zorba, X.L. Mao, R.E. Russo. Ultrafast laser induced breakdown spectroscopy for high spatial resolution chemical analysis. *Spectrochimica Acta Part B: Atomic Spectroscopy*, 66(2) (2011), 189-192.
- [14] H. Huang, L.-M. Yang, J. Liu, Qualitative assessment of laser-induced breakdown spectra generated with a femtosecond fiber laser, *Appl. Opt.* 51 (2012), 8669–8676.
- [15] H. Huang, L.-M. Yang, J. Liu. Femtosecond fiber-laser-based, laser-induced breakdown spectroscopy. *Proc. SPIE* 8358 (2012), 835817.
- [16] J.-F. Y. Gravel, P. Bouchard, M. Sabsabi, F. R. Doucet. Evaluation of a compact high power pulsed fiber laser source for laser-induced breakdown spectroscopy. *J. Anal. At. Spectrom.*, 26 (2011), 1354-1361.
- [17] L. V. Zhigilei, Z. Lin, D. S. Ivanov. Atomistic Modeling of Short Pulse Laser Ablation of Metals: Connections between Melting, Spallation, and Phase Explosion. *J. Phys. Chem. C*, 113 (2009), 11892-11906.
- [18] C. Wu, L. V. Zhigilei. Microscopic mechanisms of laser spallation and ablation of metal targets from large-scale molecular dynamics simulations. *Appl. Phys. A*, 114 (2014), 11-32.
- [19] M. Birnbaum. Semiconductor Surface Damage Produced by Ruby Lasers. *J. Appl. Phys.* 36 (1965), 3688.
- [20] J. E. Sipe. J. F. Young, J. S. Preston, H. M. van Driel. Laser-induced periodic surface structure. *Phys. Rev. B*, 27 (1982), 1141-1154.
- [21] G. Miyaji, K. Miyazaki. Role of multiple shots of femtosecond laser pulses in periodic surface nanoablation. *Appl. Phys. Lett.* 103 (2013), 071910.
- [22] J. Bonse, J. Krüger. Pulse number dependence of laser-induced periodic surface structures for femtosecond laser irradiation of silicon. *J. Apply. Phys.* 108 (2010), 034903.
- [23] S. Höhma, A. Rosenfeld, J. Krüger, J. Bonse. Area dependence of femtosecond laser-induced periodic surface structures for varying band gap materials after double pulse excitation. *Applied Surface Science*, 278 (2013), 7-12.

- [24] J. Bonse, S. Baudach, J. Krüger, W. Kautek, M. Lenzner. Femtosecond laser ablation of silicon–modification thresholds and morphology. *Appl. Phys. A*, 74 (2002), 19-25.
- [25] B. Nie, G. Parker, V.V. Lozovoy, M. Dantus. Energy scaling of Yb fiber oscillator producing clusters of femtosecond pulses. *Optical Engineering*, 53(5) (2014), 051505-051505.
- [26] T.C. Gunaratne, M. Kangas, S. Singh, A. Gross, M. Dantus. Influence of bandwidth and phase shaping on laser induced breakdown spectroscopy with ultrashort laser pulses. *Chemical physics letters*, 423(1) (2006), 197-201.
- [27] T.C. Gunaratne, X. Zhu, V.V. Lozovoy, M. Dantus. Influence of the temporal shape of femtosecond pulses on silicon micromachining. *J. Appl. Phys.* 106 (2009), 123101.
- [28] C. Momma, S. Nolte, B.N. Chichkov, F. v. Alvensleben, A. Tünnermann. Precise laser ablation with ultrashort pulses. *Applied surface science*, 109 (1997), 15-19.
- [29] X. Zeng, X.L. Mao, R. Grief, R.E. Russo. Experimental investigation of ablation efficiency and plasma expansion during femtosecond and nanosecond laser ablation of silicon. *J. Appl. Phys. A*. 80 (2005), 237-241.
- [30] P. Poízka, B. Klessen, J. Kaiser, I. Gornushkin, U. Panne, J. Riedel. High repetition rate laser-induced breakdown spectroscopy using acousto-optically gated detection. *Review of Scientific Instruments*. 85 (2014), 073104.
- [31] M. Hoehse, I. Gornushkin, S. Merka, U. Panne. Assessment of suitability of diode pumped solid state lasers for laser induced breakdown and Raman spectroscopy. *J. Anal. Atom. Spectrometry*. 26 (2011), 414-424.
- [32] S.M. Clegg, E. Sklute, M.D. Dyar, J.E. Barefield, R.C. Wiens. Multivariate analysis of remote laser-induced breakdown spectroscopy spectra using partial least squares, principal component analysis, and related techniques. *Spectrochimica Acta Part B: Atomic Spectroscopy*, 64(1) (2009), 79-88.

Spectrochimica Acta Part B

Highlights

- We performed LIBS using a unique ultrafast fiber laser oscillator producing clusters of femtosecond pulses at 2 MHz.
- We found the LIBS threshold to be lower than the ablation threshold for single femtosecond laser pulses.
- The high repetition rate leads to very stable LIBS signals.
- We introduce a model for the LIBS threshold that leads to more accurate determination of threshold values.
- We provide results for a number of different solid samples.
- The new setup could lead to the design of very compact (portable) and femtosecond-LIBS setups.